Original Article

Biomechanical evaluation of sagittal maxillary internal distraction osteogenesis in unilateral cleft lip and palate patient and noncleft patients

A three-dimensional finite element analysis

Sultan Olmez[a]; Servet Dogan[b]; Mahmut Pekedis[c]; Hasan Yildiz[d]

ABSTRACT

Objective: To compare the pattern and amount of stress and displacement during maxillary sagittal distraction osteogenesis (DO) between a patient with unilateral cleft lip and palate (UCLP) and a noncleft patient.

Materials and Methods: Three-dimensional finite element models for both skulls were constructed. Displacements of the surface landmarks and stress distributions in the circummaxillary sutures were analyzed after an anterior displacement of 6 mm was loaded to the elements where the inferior plates of the distractor were assumed to be fixed and were below the Le Fort I osteotomy line.

Results: In sagittal plane, more forward movement was found on the noncleft side in the UCLP model (−6.401 mm on cleft side and −6.651 mm on noncleft side for the central incisor region). However, similar amounts of forward movement were seen in the control model. In the vertical plane, a clockwise rotation occurred in the UCLP model, whereas a counterclockwise rotation was seen in the control model. The mathematical UCLP model also showed higher stress values on the sutura nasomaxillaris, frontonasalis, and zygomatiomaxillaris on the cleft side than on the normal side.

Conclusions: Not only did the sagittal distraction forces produce advancement forces at the intermaxillary sutures, but more stress was also present on the sutura nasomaxillaris, sutura frontonasalis, and sutura zygomaticomaxillaris on the cleft side than on the noncleft side. (*Angle Orthod.* 2014;84:815–824.)

KEY WORDS: Finite element analysis; Maxillary advancement; Distraction osteogenesis; UCLP

INTRODUCTION

Patients with cleft lip and palate (CLP) and maxillary hypoplasia usually present with a collapsed maxillary dental arch and impaired forward and downward growth of the maxilla as a result of congenital reduction in midfacial growth and scar tissue from the early surgical repair of CLP.[1,2] These problems often require both orthodontics and orthognathic surgery, such as Le Fort I osteotomy[3] or distraction osteogenesis (DO).[4] DO is a biological process involving the formation of new bone between viable bone segments that are gradually separated by incremental traction. The standard osteotomy used for the DO of the hypoplastic maxilla is Le Fort I. An advancement of more than 10 mm in patients with no cleft and 6 mm in patients with CLP is beyond the limit of Le Fort osteotomy, and in such cases DO for advancement of the maxilla can be used.[5–8]

Three-dimensional (3D) finite element model (FEM) analysis is a helpful mathematical instrument for use in orthodontics and can determine the amount of stress, strain, and displacement in the maxillofacial complex after different loading conditions of force.[9] The aim of this study was to determine the biomechanical effects of sagittal maxillary distraction osteogenesis using FEM analysis in a unilateral cleft lip and palate (UCLP)

[a] Private Practice, Izmir, Turkey.
[b] Professor, Department of Orthodontics, School of Dentistry, Ege University, Izmir, Turkey.
[c] Research Assistant, Department of Mechanical Engineering, Faculty of Engineering, Ege University, Izmir, Turkey.
[d] Professor, Department of Mechanical Engineering, Faculty of Engineering, Ege University, Izmir, Turkey.
Corresponding author: Sultan Olmez, DDS, PhD, Kazimdirik M. Fatif C. Rayman Apt. No: 39/7 Bornova, Izmir, Turkey (e-mail: sultanolmez@gmail.com)

Accepted: December 2013. Submitted: August 2013.
Published Online: February 19, 2014

Table 1. Material Properties Used in the Finite Element Model Analysis

Material	Young's Modulus, MPa	Poisson's Ratio
Cortical bone	13,700	0.3
Trabecular bone	1370	0.3
Callus	8	0.3

patient and to compare the results with those of a noncleft patient.

MATERIALS AND METHODS

A 20-year-old, nonsyndromic male patient with complete UCLP on the left side who had not had alveolar bone grafting and a 21-year-old male patient with no cleft needing more than 10 mm of maxillary advancement were chosen for this study. Both patients had maxillary hypoplasia, with a normal vertical growth pattern and posterior and anterior crossbite, and both needed sagittal maxillary advancement with DO. The principles outlined in the Declaration of Helsinki were followed.

The computed tomography (CT) DICOM data were obtained preoperatively at 1-mm intervals with spiral movements along the body axis to enable high geometric accuracy. The DICOM data were imported into MIMICS 10.01 software, and surface mesh was built up. AutoCAD® 2010 software (AutoCAD® 2010, 2009 Autodesk Inc, San Francisco, Calif) was used to eliminate the unwanted or distorted sections, such as mandibular bone and cervical vertebrae. FEM analysis was performed using ANSYS v.11.0 (ANSYS Inc, Houston, Pa).

The UCLP model consisted of approximately 650,000 tetrahedral elements and 900,000 nodes, whereas the noncleft model consisted of approximately 900,000 elements and 1,200,000 nodes. SOLID 92 was well suited to modeling the irregular meshes as a result of its quadratic displacement behavior. Material properties of the cortical bone (except maxillary cortical bone), trabecular bone, and the callus tissue were selected according to the published literature and are shown in Table 1.[10,11] The materials were assumed to be linear, isotropic, and homogeneous, except in the case of the maxillary cortical bone. The elements along the osteotomy line were defined as callus tissue, and the material properties of the callus tissue were selected. Maxillary cortical bone material properties were defined by Peterson et al.[12] in 2006 for 15 different regions, so their elastic modulus, shear modulus, and Poisson's ratio were used.

Boundary conditions were defined at the foramen magnum, in the area where the superior plates of the distractor were assumed to be fixed at the zygomatic buttress. To prevent rotational movements due to the bending forces, fixation was imposed on the nodes along the upper side of the cranial vault (Figure 1). A Le Fort I osteotomy line was simulated according to the real surgical procedure, and the elements selected for the osteotomy line were defined as callus tissue at 7 days of the latency period. In this study, it was assumed that the plates of the distractors were placed below this osteotomy line. The elements were selected by a surgeon referring to the plates of the distractors. Therefore, anterior displacements of 1 and 6 mm, corresponding to two turns and 12 turns of the distractor screw, respectively, were loaded perpendicular to these elements (Figure 1).

The displacement patterns and the von Mises stress distribution patterns in selected regions of the skull were analyzed, undergoing 1- and 6-mm advancements, respectively, using the FEM.

RESULTS

Tables 2 and 3 show the 3D pattern of displacement and von Mises stress distributions at different anatomic parts on the maxillary bone. Displacement and stress distributions of the maxillary anatomic structures are shown in Figures 2–5.

Displacements in the Sagittal Plane (u_y)

UCLP model. In the sagittal plane, the maximum "y" displacement was −6.65 mm at point A, indicating that this portion of the maxillary bone moved forward. Anterior nasal spine (ANS) moved 6.24 mm anteriorly. In the cleft area, maximum forward displacements were observed at the central incisor (−6.401 mm), canine (−6.311 mm), molar (−5.627 mm), and retromolar (−5.258 mm) regions. However, in the noncleft area the displacements were different and showed more forward movement than was noted on the cleft side. The displacement values were −6.651 mm, −6.410 mm, −5.929 mm, and −5.542 mm, respectively, for these regions.

Control model. The displacements in the sagittal plane were similar on the right and the left sides of the maxillary bone, as shown in Figure 2b, indicating more symmetrical movements forward.

Displacements in the Transverse Plane (u_x)

UCLP model. In the transverse plane, the UCLP model showed asymmetrical displacement distributions at dento-alveolar regions and in the lateral nasal area. On the cleft side, the maxillary central incisor and canine regions showed outward displacement, whereas molar and retromolar regions showed inward displacements. On the noncleft side, the amount of the outward movement at the selected regions decreased posteriorly. The lateral nasal walls also

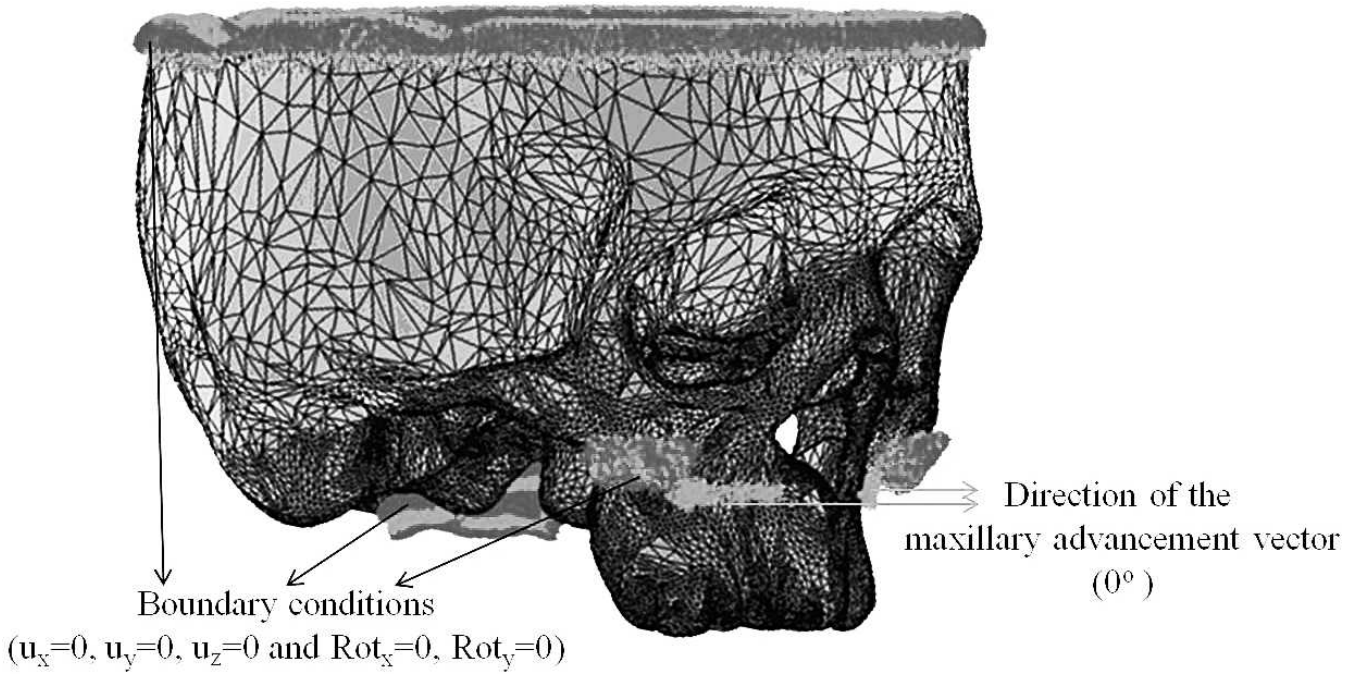

Figure 1. Three-dimensional finite element model of a patient with UCLP. Black arrows represent the boundary conditions at the foramen magnum, the upper side of the cranial vault, and the zygomatic buttress, where the superior plates of the distractor are assumed to be fixed. Red arrows represent the direction of the maxillary advancement vector.

moved outward on both cleft and noncleft sides, but more lateral movement was detected on the noncleft side.

Control model. Similar transverse displacements were found on both sides of the maxillary halves, and all movements indicated expansion.

Displacements in the Vertical Plane (u_y)

UCLP model. The vertical changes in the UCLP model were mostly located in the dento-alveolar regions. Point A and ANS moved downward (−0.355 mm and −0.148 mm, respectively). Superior movements (0.192–0.611 mm) were seen at superior portions of the lateral nasal walls. More superior displacement was seen at the infraorbital margin on the cleft side than on the noncleft side (0.114 mm and 0.006 mm, respectively). As a result of the forward advancement, the maxillary bone rotated clockwise in the UCLP model, meaning more downward displacement occurred in the incisor region than in the posterior regions.

Control model. Although most maxillary distraction should create a clockwise rotation of the maxilla clinically, the vertical changes for the control model in the dento-alveolar regions showed a counterclockwise rotation of the maxilla.

von Mises Stress Distribution

UCLP model. The highest stress levels were observed bilaterally at the foramen infraorbitalis and at the infraorbital margins in the UCLP model. On the cleft side, higher stress values were exhibited on the sutura nasomaxillaris, sutura frontonasalis, and zygomaticomaxillaris than on the noncleft side.

Control model. In the control model, the maximum von Mises stress levels were observed at the infraorbital margins, as was the case with the UCLP model. Relatively high stress values were also found at the sutura frontomaxillaris, sutura nasomaxillaris, and foramen infraorbitalis.

DISCUSSION

Most surgeons accept that advancement of more than 6 mm in patients with CLP and more than 10 mm in noncleft patients is beyond the present limit of orthognathic surgery and can only be achieved by DO.[6,7]

The FEM is a valid and noninvasive method that provides useful results with which to predict various parameters of the complex biomechanical behavior of the human maxillofacial complex.[13] Although many clinical research studies and case reports have been published about sagittal maxillary advancement with DO, there is no article concentrated on comparing the biomechanical effects associated with this procedure in patients with and without clefts. In 2011 Olmez et al.[14] investigated the effects of DO in a patient with CLP using FE analysis, preliminary to the current study. Therefore, in the present study, the biomechanical

Table 2. Three-Dimensional (3D) Pattern of Displacement and von Mises Stress Distributions at Different Anatomic Structures on the Maxillary Bone for Unilateral Cleft Lip and Palate (UCLP) Finite Element Model[a]

	u_x, mm		u_y, mm		u_z, mm		von Mises, MPa	
	Cleft Side	Noncleft Side	Cleft Side	Noncleft Side	Cleft Side	Noncleft Side	Cleft Side	Noncleft Side
1	−0.1501		−0.0900		0.0382		4.0233 (min) 29.4375 (max)	
2	−0.0058		−0.0909		−0.0394		3.2468 (min) 14.4280 (max)	
3	−0.0179	−0.0303	−0.0610	−0.0219	−0.0181	−0.0128	2.1800 (min) 20.7355 (max)	2.3807 (min) 21.4355 (max)
4	−0.0085	−0.0151	−0.1255	−0.1306	−0.0050	−0.0040	0.8590 (min) 7.7363 (max)	2.0673 (min) 14.7657 (max)
5	−0.0170	−0.0152	−0.1298	−0.1471	−0.0680	−0.0576	0.8487 (min) 7.3977 (max)	0.8368 (min) 11.4103 (max)
6	−0.0146	−0.0155	−0.5029	−0.4147	−0.0114	−0.0210	1.8173 (min) 39.4102 (max)	1.5162 (min) 27.2578 (max)
7	0.0274	0.0208	−0.0385	−0.0029	−0.0157	−0.0190	0.2313 (min) 6.1803 (max)	0.7508 (min) 6.7335 (max)
8	−0.0277	−0.0380	−0.0076	−0.0177	−0.0277	−0.0166	0.3597 (min) 15.5780 (max)	0.0032 (min) 5.6297 (max)
9	0.1178	0.3790	−0.9440	−0.7150	−0.0840	−0.0580	10.5433 (min) 63.2067 (max)	23.0270 (min) 24.3883 (max)
10	−0.0710	−0.0170	−0.0240	−0.0450	0.1140	0.0055	2.4767 (min) 72.3533 (max)	0.9877 (min) 2.7645 (max)
11	−0.0145	−0.0100	−0.0796	−0.0800	−0.0933	0.0700	0.0005 (min) 0.0046 (max)	0.6417 (min) 3.1900 (max)
12	–	−1.0650	–	−6.4510	–	−0.3513	–	0.4387 (min) 2.7093 (max)
13	0.6320	−0.6750	−6.3110	−6.3700	−1.0060	−0.8320	0.4503 (min) 18.1698 (max)	4.7182 (min) 14.3545 (max)
14	−0.6467	−0.5130	−5.6270	−5.9290	−0.7678	−0.7890	0.3567 (min) 9.9780 (max)	1.6267 (min) 18.4167 (max)
15	−0.7127	−0.0629	−5.2580	−5.5420	−0.8020	−0.9880	3.5133 (min) 13.7467 (max)	0.9867 (min) 14.2583 (max)
16	1.1040	−1.3760	−1.810	−2.233	0.1920	0.6110	0.1232 (min) 38.6750 (max)	6.4376 (min) 34.4628 (max)
17	–	1.7097	–	−6.4650	–	−0.3555	–	0
18	0.2644		−6.2370		−0.1478		1.4216 (min) 8.2650 (max)	
19	−0.2982		−6.6510		−0.3052		0.2030 (min) 2.7467 (max)	

[a] 1, sutura internasalis; 2, synchondrozis spheno-occipitalis; 3, sutura zygomaticomaxillaris; 4, sutura frontonasalis; 5, frontomaxillaris; 6, sutura nasomaxillaris; 7, sutura temporozygomatica; 8, sutura frontozygomatica; 9, foramen infraorbitalis; 10, infraorbital margin; 11, supraorbital margin; 12, central incisor region at alveolar bone; 13, canine region at alveolar bone; 14, molar region at alveoalar bone; 15, retromolar region at alveolar bone; 16, lateral nasal wall; 17, tip of the upper central incisor; 18, anterior nasal spina (ANS); and 19, A point.

Table 3. Three-Dimensional (3D) Pattern of Displacement and von Mises Stress Distributions at Different Anatomic Structures on the Maxillary Bone for Noncleft Finite Element Model[a]

	u_x, mm		u_y, mm		u_z, mm		von Mises, MPa	
	Right Side	Left Side	Right Side	Left Side	Right Side	Left Side	Right Side	Left Side
1	−0.1306		−0.0761		0.0282		2.0259 (min) 4.9262 (max)	
2	−0.0137		−0.0819		−0.0374		4.2061 (min) 12.4593 (max)	
3	−0.0755	−0.1871	−0.0966	−0.1837	−0.2135	−0.2913	1.642 (min) 31.127 (max)	0.5356 (min) 29.275 (max)
4	−0.0769	−0.0839	−0.1194	−0.1412	0.2268	0.2046	1.948 (min) 8.364 (max)	1.776 (min) 5.516 (max)
5	−0.0785	−0.0794	−0.2815	−0.3296	0.0857	0.0802	2.165 (min) 28.01 (max)	1.246 (min) 26.418 (max)
6	−0.0384	−0.1799	−0.3708	−0.3644	0.2486	0.3294	7.538 (min) 30.546 (max)	7.386 (min) 29.331 (max)
7	−0.2177	−0.1902	−0.1243	−0.1074	−0.2466	−0.2345	1.231 (min) 7.803 (max)	0.4113 (min) 6.35 (max)
8	−0.0375	−0.0270	−0.0392	−0.1943	−0.0222	−0.0438	0.4829 (min) 7.312 (max)	0.548 (min) 8.045 (max)
9	−0.2210	−0.0757	−0.1241	−0.3179	−0.1906	−0.0909	10.234 (min) 24.345 (max)	8.9872 (min) 21.357 (max)
10	−0.0382	−0.0885	−0.5244	−0.4395	−0.2066	−0.3253	2.556 (min) 21.411 (max)	1.7419 (min) 22.296 (max)
11	−0.0197	−0.0078	−0.3396	−0.4338	−0.1402	−0.1824	2.567 (min) 12.02 (max)	2.9462 (min) 13.551 (max)
12	−0.0040	0.0027	−6.2220	−6.3200	1.4133	1.4644	1.253 (min) 10.869 (max)	1.983 (min) 14.674 (max)
13	−0.0260	0.0162	−6.2140	−6.2220	0.1289	0.0999	3.096 (min) 27.648 (max)	4.746 (min) 30.164 (max)
14	−0.2820	0.2548	−6.1460	−6.1200	−0.2581	−0.3164	10.518 (min) 34.327 (max)	9.965 (min) 32.804 (max)
15	−0.2962	0.2759	−5.0880	−5.0360	−0.2028	−0.2691	4.184 (min) 6.42 (max)	4.499 (min) 5.94 (max)
16	−0.6786	0.4482	−1.7538	−1.8127	−0.0436	−0.0398	3.2232 (min) 35.8291 (max)	2.7382 (min) 33.7620 (max)
17	−0.5478	−0.5551	−6.7788	−6.7756	0.7866	0.7988	0	0
18	−0.2721		−6.2280		0.2351		0.9231 (min) 5.7256 (max)	
19	−0.2654		−6.4394		0.4210		0.0178 (min) 2.3241 (max)	

[a] 1, sutura internasalis; 2, synchondrozis spheno-occipitalis; 3, sutura zygomaticomaxillaris; 4, sutura frontonasalis; 5, frontomaxillaris; 6, sutura nasomaxillaris; 7, sutura temporozygomatica; 8, sutura frontozygomatica; 9, foramen infraorbitalis; 10, infraorbital margin; 11, supraorbital margin; 12, central incisor region at alveolar bone; 13, canine region at alveolar bone; 14, molar region at alveoalar bone; 15, retromolar region at alveolar bone; 16, lateral nasal wall; 17, tip of the upper central incisor; 18, anterior nasal spina (ANS); and 19, A point.

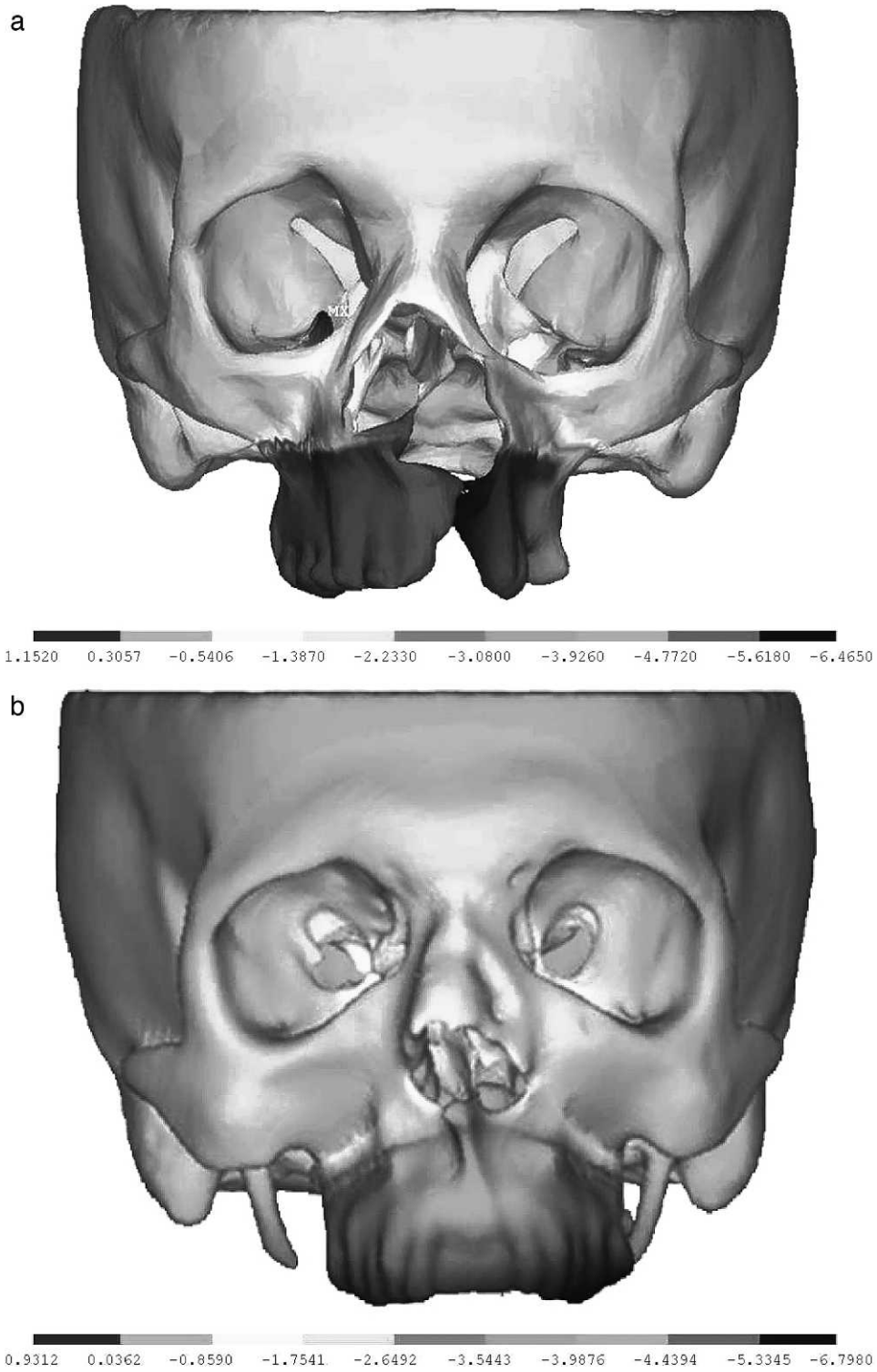

Figure 2. Displacement distribution in the sagittal plane after 6 mm of maxillary advancement. (a) for the UCLP model; and (b) for the control model.

effects of internal maxillary advancement using DO were analyzed both in UCLP and noncleft FEMs.

In 1994, Miyasaka-Hiraga et al.[15] had an FEM of the skull that consisted of 1776 elements; the model of Iseri et al.[16] in 1998 consisted of 2349 individual elements. The geometric precision increased further in the papers of Holberg et al.,[17,18] who introduced FEMs of the skull with approximately 31,000 elements for rapid maxillary expansion therapy simulation and 54,000 elements for maxillary protraction simulation

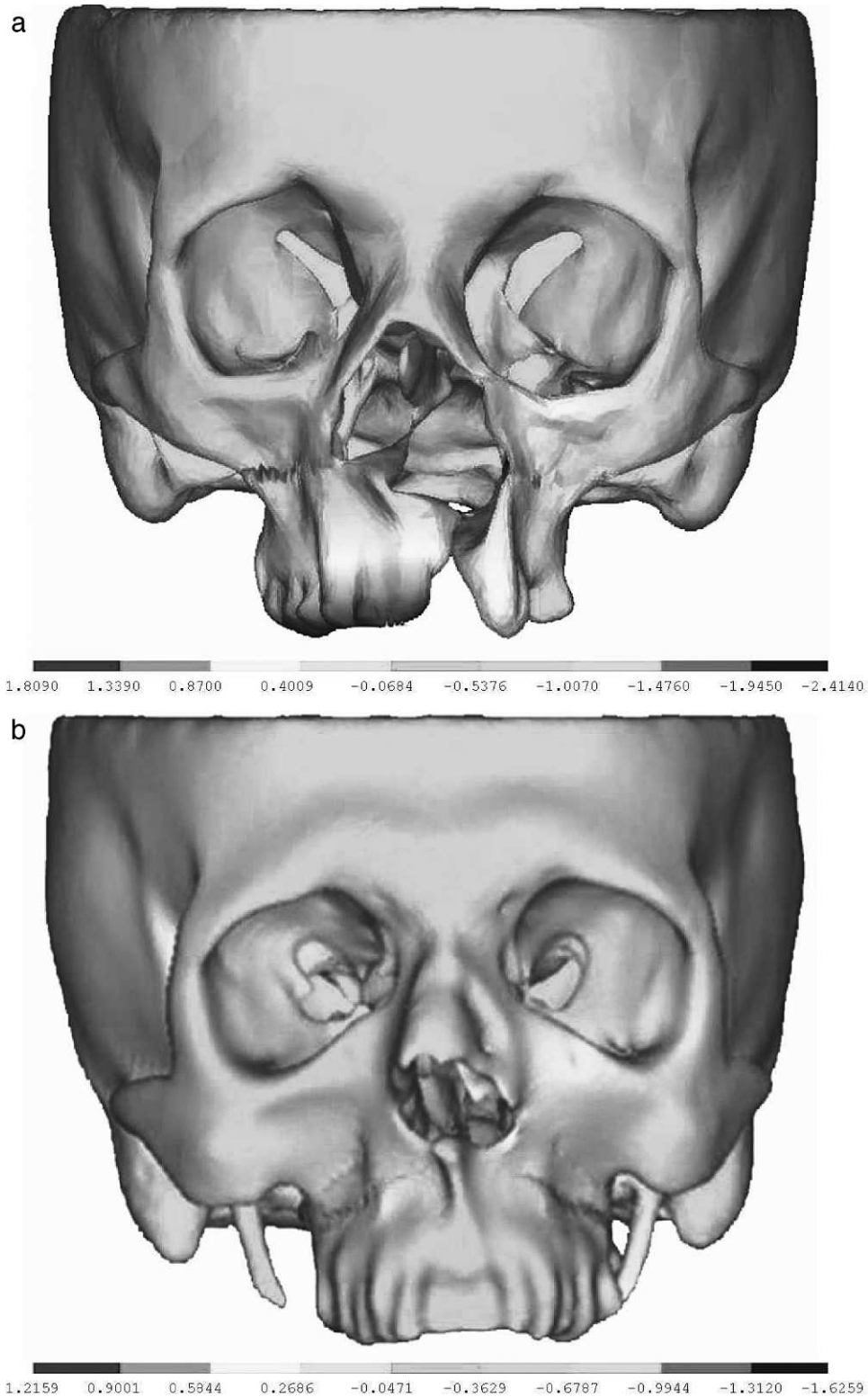

Figure 3. Displacement distribution in the transverse plane after 6 mm of maxillary advancement. (a) for the UCLP model; and (b) for the control model.

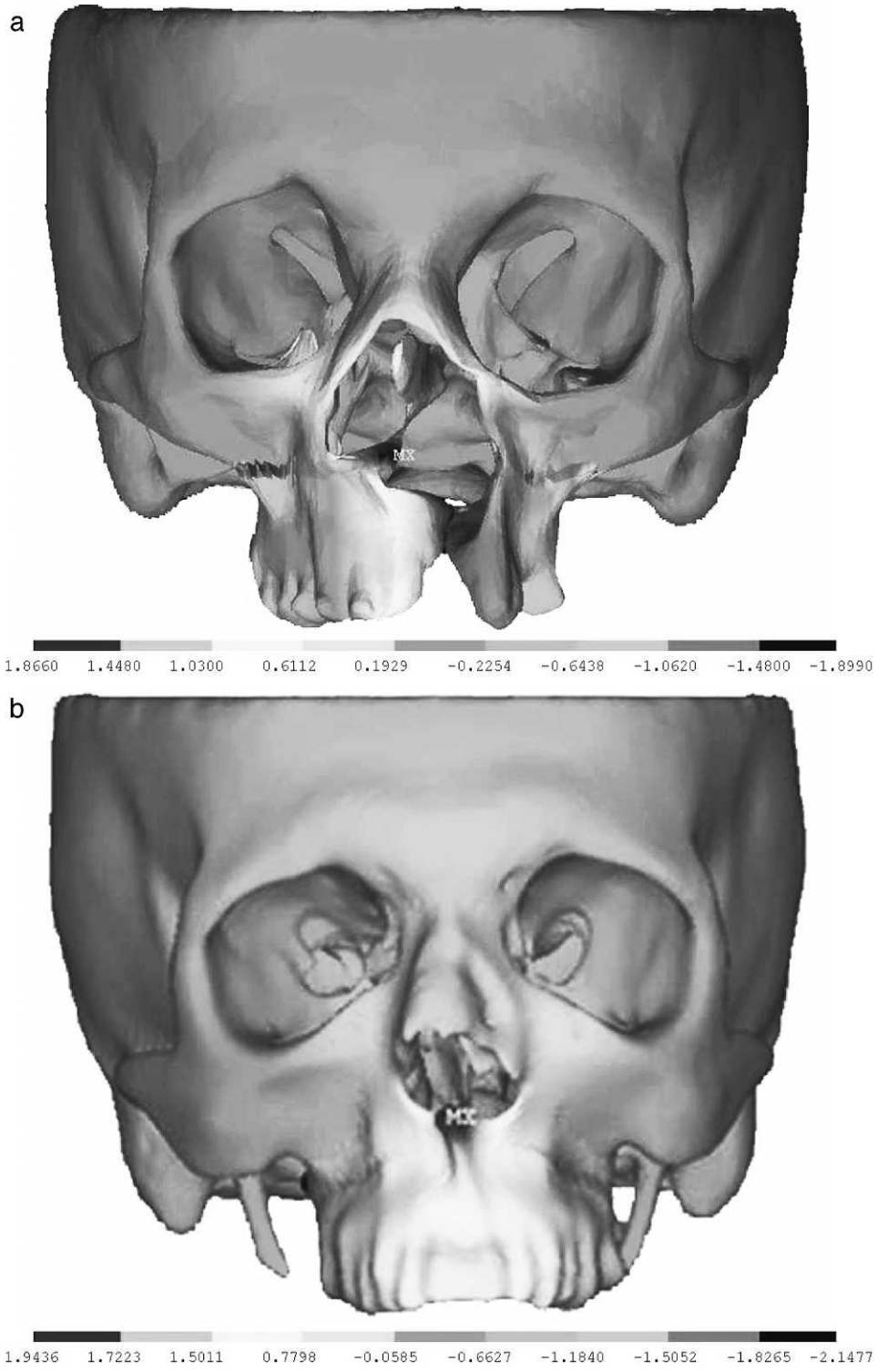

Figure 4. Displacement distribution in the vertical plane after 6 mm of maxillary advancement. (a) for the UCLP model; and (b) for the control model.

in 2007. Compared to the FEMs of the skull available until now, the number of elements increased and the anatomical differentiations were improved in this study.The results of FEM analysis are highly dependent on the quality of the constructed models.[19] Therefore, the models must be developed to approximate as closely as possible the real object in various aspects.[16] In FEM studies the material properties of the skull are generally assumed to be homogeneous, isotropic, and linearly elastic. However, in the present

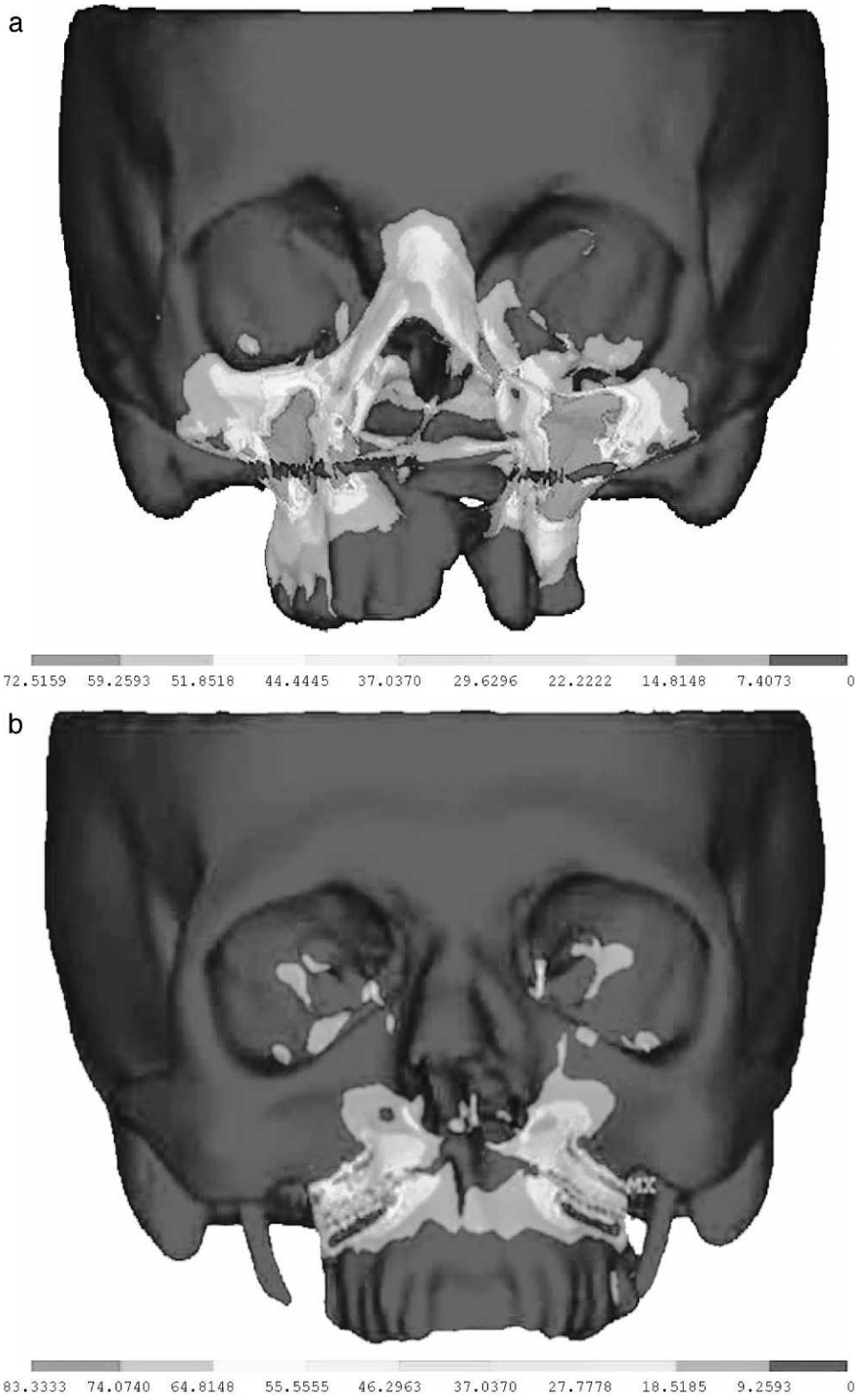

Figure 5. The magnitude and distribution of the von Mises stresses after 1 mm of maxillary advancement. (a) for the UCLP model; and (b) for the control model.

study maxillary cortical bone material properties were defined to be orthotropic, as described by Peterson et al.[12] This made the problem even more complex but rendered the results more reliable.

The displacement distribution in the sagittal plane was asymmetric in the UCLP model. The different amounts of antero-posterior movements after sagittal maxillary distraction could have been a result of the ungrafted alveolar region in this model. In the control model, since the maxillary arch was as a unit with no cleft history, similar sagittal displacements were observed on both sides. According to these findings, it would be important to perform secondary alveolar bone grafting at the proper age to stabilize the maxillary arch as one segment, especially if further treatment procedures are needed. However, the amount of maxillary advancement can be different on the two sides, for example, if greater advancement was needed on the cleft side.

In this study, the maxilla rotated in a clockwise direction after maxillary advancement. On the cleft side, more inferior displacements were observed. However, in the control model, the maxilla rotated in a counterclockwise direction. Baek et al.[20] also found 3° of counterclockwise rotation in one of their study groups and concluded that this rotation may be a result of vector control problems in maxillary distraction osteogenesis during their early experience. On the other hand, this counterclockwise rotation induced clockwise rotation of the mandible through the wedge effect, and, therefore, point B moved backward and downward in direction. In the present study, after the Le Fort I osteotomy was performed on the FEMs, an anterior displacement was defined at the elements placed below the osteotomy line, where the inferior plates of the internal maxillary distractors were assumed to be fixed. So the displacement vector was perpendicular to these elements. The different pattern of the maxillary rotation in these FEMs may have resulted from both the different anatomical structures of the patient models and the displacement vector acting on these elements. Therefore, changing the force vector to a more downward direction might be recommended to minimize the unwanted counterclockwise rotation tendency of the nasomaxillary complex.[20,21]

Previous literature[22–24] has shown that after maxillary advancement achieved by DO, patients with upper airway obstruction gain airway sufficiency. In the present study using 3D CT data and FEMs, we did not include the soft tissue and the mandibular bone in order to minimize the duration of the FEM analysis. Therefore, the amount of transverse change at the lateral nasal walls was measured and was found to have expanded in both of the FEMs. In accordance with lateral nasal width increase, nasal airway could be improved after DO in the maxilla.

In this study, the highest stress values were observed at the foramen infraorbitalis and the infraorbital margins in the UCLP model. In the control model, the maximum von Mises stress levels were observed at the infraorbital margins, as was the case with the UCLP model. It has been observed clinically that some patients felt pressure under the eyes, around the lateral nasal walls, and generally throughout the face during and after the distractor activations. These anatomical landmarks coincide with the area of high-stress distribution in the present study. Moreover, the frontonasal region is also one of the most common regions in which pain is detected during and after the screw activations. Parallel to the clinical findings, the mathematical UCLP model presented greater stress values on the sutura nasomaxillaris, sutura frontonasalis, and zygomatiomaxillaris on the cleft side than on the normal side. Holberg et al.[18] also found high stresses at the sutura nasomaxillaris, frontonasalis, frontomaxillaris, sphenotemporalis, and sphenofrontalis in a study in which they examined the strain in the sutures of the midface and the cranial base with maxillary protraction therapy. Lee and Baek[25] found the maximum von Mises stresses at the pterygomaxillary, zygomaticotemporal, zygomaticomaxillary, and frontonasal sutures, in descending order, after maxillary protraction using miniplates placed at the infrazygomatic crest and the lateral nasal wall.

The biomechanical reactions elucidated in this study may help the surgeon and the orthodontist to understand better the therapeutic effects of internal maxillary DO on the basal bones and sutures of the craniofacial system.

CONCLUSIONS

- The noncleft side of the UCLP FEM showed more anterior displacement than did the cleft side, which can result from the asymmetrical skeletal development of the anatomical structures. The control FEM showed more symmetrical anterior displacements when compared to the UCLP FEM.
- The results of the present study using the FEM of a UCLP patient indicated that the sagittal distraction forces produced not only advancement forces at the intermaxillary sutures but also higher stress values at the sutura nasomaxillaris, sutura frontonasalis, and sutura zygomaticomaxillaris on the cleft side compared to the noncleft side.
- However, in the FEM of the noncleft patient, relatively high stress values were found at the sutura frontomaxillaris and sutura nasomaxillaris, similar to the findings on the noncleft side of the UCLP FEM.

- Since the clinical effectiveness of maxillary DO is highly dependent on the presence of scar tissue in patients with CLP, it would be helpful to incorporate this soft tissue into future models, despite the added difficulty of building a more detailed FEM.

REFERENCES

1. Ross RB. Treatment variables affecting facial growth in complete unilateral cleft lip and palate. *Cleft Palate J*. 1987; 24:5–77.
2. Cheung LK, Chua HDP. A meta-analysis of cleft maxillary osteotomy and distraction osteogenesis. *Int J Oral Maxillofac Surg*. 2006;35:14–24.
3. Adlam DM, Yau CK, Banks P. A retrospective study of the stability of midface osteotomies in cleft lip and palate patients. *Br J Oral Maxillofac Surg*. 1989;27:265–276.
4. Cohen SR, Corrigan MBA, Wilmot J, Trotman CA. Cumulative operative procedures in patients aged 14 years and older with unilateral or bilateral cleft lip and palate. *Plast Reconstr Surg*. 1995;96:267–271.
5. Saelen R, Tornes K, Halse A. Stability after Le Fort I osteotomy in cleft lip and palate patients. *Int J Adult Orthod Orthognath Surg*. 1998;13:317–323.
6. Molina F, Monasterio F, Aguliar M. Maxillary distraction: aesthetic and functional benefits in cleft lip-palate and prognathic patients during mixed dentition. *Plast Reconstr Surg*. 1998;101:951–963.
7. Costa F, Robiony M, Politi M. Stability of Le Fort I osteotomy in maxillary advancement: review of the literature. *Int J Adult Orthod Orthognath Surg*. 1999;14:207–213.
8. Yu H, Wang X, Fang B, Shen SG. Comparative study of different osteotomy modalities in maxillary distraction osteogenesis for cleft lip and palate. *J Oral Maxillofac Surg*. 2012;70:2641–2647.
9. Ozan F, Yıldız H, Bora OA, Pekedis M, Coşkun GA, Göre O. The effect of head trauma on fracture healing: biomechanical testing and finite element analysis. *Acta Orthop Traumatol Turc*. 2010;44:313–321.
10. Tanne K, Hiraga J, Kakiuchi K, Yamagata Y, Sakuda M. Biomechanical effect of anteriorly directed extraoral forces on the craniofacial complex: a study using the finite element method. *Am J Orthod Dentofacial Orthop*. 1989;95: 200–207.
11. Hiraga MJ, Tanne K, Nakamura S. Finite element analysis for stresses in the craniofacial sutures produced by maxillary protraction forces applied at the upper canines. *Br J Orthod*. 1994;21:343–348.
12. Peterson J, Wang Q, Dechow PC. Material properties of the dentate maxilla. *Anat Rec Part A*. 2006;288A:962–972.
13. Vollmer D, Meyer U, Joos U, Vegh A, Piffko J. Experimental and finite element study of a human mandible. *J Craniomaxillofac Surg*. 2000;28:91–96.
14. Olmez S, Doğan S, Pekedis M, Yildiz H. The evaluation of maxillary advancement technique using internal distraction osteogenesis in unilateral cleft lip and palate patient with finite element analysis. *J Biomech*. 2011;44(suppl 1):14.
15. Miyasaka-Hiraga J, Tanne K, Nakamura S. Finite element analysis for stresses in the craniofacial sutures produced by maxillary protraction forces applied at the upper canines. *Br J Orthod*. 1994;21:343–348.
16. Iseri H, Tekkaya AE, Oztan O, Bilgic S. Biomechanical effects of rapid maxillary expansion on the craniofacial skeleton studied by the finite element method. *Eur J Orthod*. 1998;20:347–356.
17. Holberg C, Holberg N, Schwenzer K, Wichelhaus A, Rudzki-Janson I. Biomechanical analysis of maxillary expansion in CLP patients. *Angle Orthod*. 2007;77:280–287.
18. Holberg C, Mahaini L, Rudzki I. Analysis of sutural strain in maxillary protraction therapy. *Angle Orthod*. 2007;77: 586–594.
19. Pekedis M. *Structural Analysis with Meshfree Methods* [M.Sc. thesis]. Ege University, Izmir, Turkey; 2008.
20. Baek SH, Lee JK, Lee JH, Kim MJ, Kim JR. Comparison of treatment outcome and stability between distraction osteogenesis and LeFort I osteotomy in cleft patients with maxillary hypoplasia. *J Craniofac Surg*. 2007;18:1209–1215.
21. Wang D, Cheng L, Wang C, Qian Y, Pan X. Biomechanical analysis of rapid maxillary expansion in the UCLP patient. *Med Eng Physics*. 2009;31:409–417.
22. Mochida M, Ono T, Saito K, Tsuiki S, Ohyama K. Effects of maxillary distraction osteogenesis on the upper-airway size and nasal resistance in subjects with cleft lip and palate. *Orthod Craniofacial Res*. 2004;7:189–197.
23. Xu H, Yu Z, Mu X. The assessment of midface distraction osteogenesis in treatment of upper airway obstruction. *J Craniofac Surg*. 2009;20(suppl 2):1876–1881.
24. Aksu M, Taner T, Sahin-Veske P, Kocadereli İ, Konas E, Mavili ME. Pharyngeal airway changes associated with maxillary distraction osteogenesis in adult cleft lip and palate patients. *J Oral Maxillofac Surg*. 2012;70:e133–e140.
25. Lee NK, Baek SH. Stress and displacement between maxillary protraction with miniplates placed at the infrazygomatic crest and the lateral nasal wall: a 3-dimensional finite element analysis. *Am J Orthod Dentofacial Orthop*. 2012; 141:345–351.